applied optics

Instantaneous measurement of surface roughness spectra using white-light scattering projected on a spectrometer

XAVIER BUET,[1,*] MYRIAM ZERRAD,[1] MICHEL LEQUIME,[1] GABRIEL SORIANO,[1] JEAN-JACQUES GODEME,[2] JALAL FADILI,[2] AND CLAUDE AMRA[1]

[1]Aix-Marseille University, CNRS, Centrale Marseille, Institut Fresnel, Marseille, France
[2]Normandie University, ENSICAEN, CNRS, GREYC, France
*Corresponding author: xavier.buet@fresnel.fr

Received 5 October 2022; revised 9 December 2022; accepted 27 December 2022; posted 3 January 2023; published 1 February 2023

Following on from previous studies on motionless scatterometers based on the use of white light, we propose a new, to the best of our knowledge, experiment of white-light scattering that should overtake the previous ones in most situations. The setup is very simple as it requires only a broadband illumination source and a spectrometer to analyze light scattering at a unique direction. After introducing the principle of the instrument, roughness spectra are extracted for different samples, and the consistency of results is validated at the intersection of bandwidths. The technique will be of great use for samples that cannot be moved. © 2023 Optica Publishing Group under the terms of the Optica Open Access Publishing Agreement

https://doi.org/10.1364/AO.477196

1. INTRODUCTION

Scattering techniques have been widely used since several decades [1–7] to characterize surfaces of optical quality, that is, with roughnesses much less than the illumination wavelength. Scattered light can be of critical importance in numerous domains, such as for the ultimate performances of optical filters, for advanced optical systems for astronomy, space applications, or for microelectronics. For all these applications, the reduction of roughness and surface defects is a major issue, and the improvement of polishing techniques has made possible the fabrication of surfaces with roughnesses below a fraction of a nanometer [8–12]. In parallel, measurement techniques were developed to reliably detect the properties of these surfaces, and light scattering has proven a very efficient, rapid, and noninvasive method to characterize all the requested parameters [13–15]. Angle-resolved scatterometers [16–19] today allow reaching an eight-decade dynamic below a nonabsorbing Lambertian pattern, in the whole angular range and over a wide spectral region from the visible to near infrared.

In this context, many efforts were engaged to improve the sensitivity or resolution of scatterometers, or to broaden their frequency ranges, but other needs have also emerged. For instance, some samples (large pieces or pieces that cannot be displaced) cannot be moved; or are difficult to access; or do not allow to scan an angular range around them; or require fast measurements to check the quality on a production line. For all these situations, we recently proposed an original scatterometer [20,21] that is free of any mechanical movement or wavelength scan. The system works with white light (i.e., light with a wide wavelength spectrum), which is spectrally shaped to form the illumination beam, before scattering is measured at a unique direction θ_0. The wavelength shaping is performed by two gratings coupled to a spatial light modulator [22], and a feedback loop is necessary to obtain the programmable filters $T_k(\lambda)$ with λ as the wavelength. Each filter placed in front of the incident beam makes the white (broadband) scattering at direction θ_0 proportional to a roughness moment δ_k with δ_0 as the usual roughness (root-mean square of the topography) and δ_2 as the slope root-mean square of roughness. The result is a one-shot scatterometer (Fig. 1) that instantaneously provides roughness data in a specific bandwidth [20,21]. Note here that this spectral shaping scatterometer or white-light scatterometer does not provide a direct access to the surface roughness spectra $\gamma(\nu)$ which have been commonly used until now [7–16] and that identify to the modulus square of the Fourier transform of the surface topography. However, if necessary, the knowledge of all roughness moments δ_k allow to rebuild an autocorrelation function in a reduced bandwidth [20,21].

We propose here another original setup still working with white light but which is much simpler. The benefits of the previous one are retained to the extent that there is still neither mechanical movement nor wavelength scan. The principle again relies on a wavelength/angle equivalence where the two parameters (wavelength λ, angle θ) define the spatial frequency [$\nu \sim \sin(\theta)/\lambda$]. The illumination beam is again a white-light beam, but there is no spectral shaping at the system entrance.

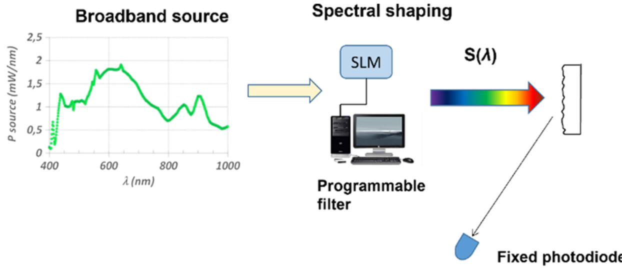

Fig. 1. Draft view of the "spectral shaping scatterometer" [20,21]. The incident beam is white light.

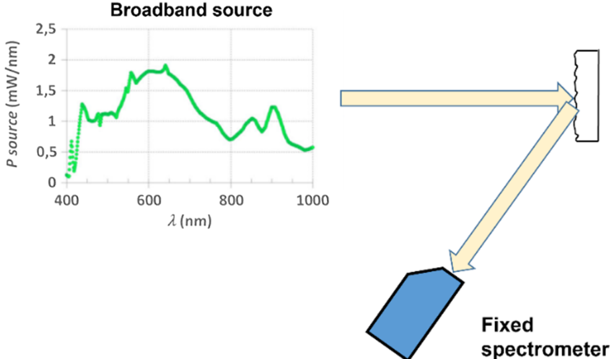

Fig. 2. Draft view of the "spectrometer scatterometer" presented in this paper. The incident beam is white light.

Actually the white scattering signal at a unique direction θ_0 is collected by an optical fiber and sent to a high-efficiency spectrometer, which allows to separate and analyze the wavelength components of scattering (Fig. 2). Each wavelength being separated by the grating inside the spectrometer is then projected on a CCD camera. This process is immediate since all the spectral components are simultaneously analyzed by the CCD matrix. Hence, each CCD pixel p_{ij} is proportional to the value γ_{ij} of the surface roughness spectrum at a specific frequency ν_{ij}. This provides, after adequate calibration, the frequency distribution of the surface roughness spectrum.

Note that the wavelength/angle equivalence has already been used to broaden the frequency window of roughness spectra, but the authors [17–19,23,24] proceeded to an angular scan, in addition to a wavelength scan obtained either with several laser lines or by placing a tunable narrowband filter in front of a supercontinuum laser. Hence, this second technique (it will be called a spectroscatterometer) is fully original in the sense that it is again free of any mechanical movement or wavelength scan. Furthermore, although both systems use white light, there are two major differences with the previous spectral shaping scatterometer:

- A passive spectrometer at the system output (case of spectroscatterometer) replaces the tunable spectral shaping at the system entrance (case of the spectral shaping scatterometer), which strongly reduces complexity and cost.
- The spectroscatterometer provides a direct access to the surface roughness spectrum unlike in the case of the spectral shaping scatterometer (which gives access to the roughness moments).

In this paper, we will present the experimental setup of the new spectroscatterometer in Section 2. Then, we discuss the calibration procedure in Section 3. Section 4 is given for the experimental results with a validation procedure discussed in Section 5. The conclusion is drawn in Section 6.

2. EXPERIMENTAL SETUP

Figure 3 shows a functional representation of the spectroscatterometer experiment. As announced, it is much less complex than the spectral shaping scatterometer presented in our previous paper, which required a wavelength shaping of the illumination beam [21]. Here, we can use the raw spectrum of any white-light source with enough power for the detection of light scattered by a polished sample. The wavelength spectrum of the white scattered intensity will be analyzed instantaneously in the detection part with the spectrometer.

The source that we use here is a supercontinuum laser NKT EXB-6 identical to the previous setup, and we still use a splitter to select only the visible part of the spectrum. This source is not polarized with an output power in the visible around 1 W. We did not add any polarizer in the setup so that we will consider only unpolarized light throughout this paper. This incident light is collimated by an achromatic reflective collimator. We added on the path of the beam a long-pass filter with a cutoff wavelength of 425 nm and a short-pass filter with a cutoff wavelength of 925 nm. Indeed, the version of our spectrometer is not equipped with any order sorting device, which is commonly used to prevent spurious effects due to the diffraction of higher orders of the grating. With these two filters, we can prevent any parasitic signal coming from this phemonenon. We also placed on the path of the beam an optical density filter OD2 to adjust the level of the light so as to avoid the saturation of the spectrometer. This density filter is necessary for the calibration step because the scattering of the Lambertian etalon sample is at a much higher level than scattering for a polished sample. This filter will be removed for low-roughness sample measurements.

A second reflective collimator collects the light scattered by the sample at a fixed angle, and a fiber optic sends the light to the detection element (the spectrometer). The fiber is at a distance of 30 cm from the sample. Its diameter is 200 µm

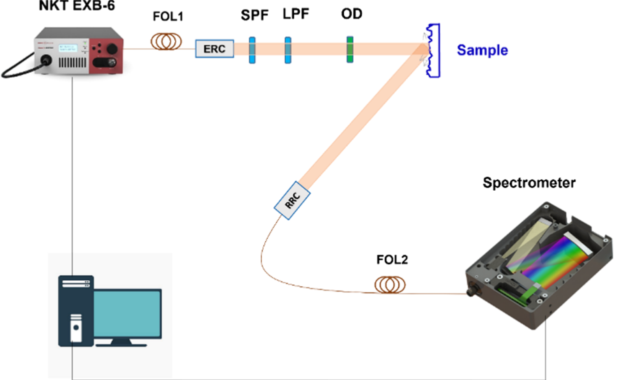

Fig. 3. Schematic of the instantaneous spectroscatterometer [(NKT EXB-6: supercontinuum laser source; FOL1: fiber-optic link 1; ERC: emission reflective collimator; SPF: short-pass filter; LPF: long-pass filter; OD: optical density filter; RRC: receiving reflective collimator; FOL2: fiber-optic link 2).

so that the solid angle is around 3.10^{-5} sr. The use of optical fibers makes the change in detector (photodiode of the previous setup is replaced by a spectrometer) very easy as we just have to change the connection of the end of the collection fiber. We used a visible-near-infrared spectrometer from WASATCH PHOTONICS with a wavelength range composed between 400 nm and 1080 nm. The separation of the wavelengths is obtained with a high transmission volume phase holographic grating, and a scientific-grade CCD with 1024 pixels of 14 µm × 14 µm performs the detection. A $f/2$ input is used to collect more light. All these elements maximize the efficiency and detectivity of this instrument.

3. CALIBRATION PROCEDURE

Although the setup shows key differences with a classical angle-resolved scatterometer (ARS), the calibration procedure still relies on a Lambertian sample at normal illumination. However, the properties of this etalon sample must be guaranteed in the whole spectral range. Its known achromatic pattern can be written as

$$I_L(\theta_0, \lambda) = \frac{[1 - A] \cos(\theta_0)}{\pi}, \tag{1}$$

where A is the slight absorption of the Lambertian and θ_0 is the angle at which we collect the scattered light on the incidence plane. Inside the spectrometer, the white scattered light at direction θ_0 is diffracted by the grating, and then each pixel detects a part of the spectrum composed in a small interval $\Delta\lambda$ determined by the size of the pixel and the characteristics of the grating. We can, thus, write the signal on each pixel p_{ij} as

$$S_L(\theta_0, \lambda_{ij}) = \Delta\Omega \ \cos\theta_0 \frac{1 - A}{\pi} \int_{\Delta\lambda} \alpha_g(\theta_0, \lambda) K(\lambda) F(\lambda) \mathrm{d}\lambda, \tag{2}$$

where $\Delta\Omega$ is the solid angle of measurements for one pixel, α_g is the efficiency of the grating, K is the spectral response of the detector, and F is the power spectrum density of the source. The integration is performed around λ_{ij}. Note that actually we work on a single line ($j =$ constant) since all data are recorded on the incidence plane. We consider that the interval $\Delta\lambda$ is small enough to approximate the functions with constants in (2). In our case, we have $\Delta\lambda = 0.7$ nm, hence, this hypothesis seems reasonable. We can, then, reformulate the signal without the integration, that is,

$$S_L(\theta_0, \lambda_{ij}) = \Delta\lambda\Delta\Omega \cos\theta_0 \frac{1 - A}{\pi} \alpha_g(\theta_0, \lambda_{ij}) K(\lambda_{ij}) F(\lambda_{ij}). \tag{3}$$

Then, we consider a sample with a low roughness compared to the illumination wavelength. For this type of sample, we use the classical ARS formula of first-order scattering [7,10,25],

$$I_s(i, \theta_0, \lambda) = \gamma(i, \theta_0, \lambda) C(i, \ \theta_0, \lambda), \tag{4}$$

where γ is the roughness spectrum of the sample and C is an optical factor independent of the topography. The illumination angle is denoted as i. As for the previous sample, the detected signal on each pixel can be expressed as

$$S_s(i, \ \theta_0, \lambda_{ij}) = \Delta\Omega \int_{\Delta\lambda} \gamma(i, \theta_0, \lambda) C(i, \ \theta_0, \lambda) \times \alpha_g(\theta_0, \lambda) K(\lambda) F(\lambda) \mathrm{d}\lambda, \tag{5}$$

and with the same approximation,

$$S_s(i, \theta_0, \lambda_{ij}) = \Delta\lambda \ \Delta\Omega \ \gamma(i, \theta_0, \lambda_{ij}) C(i, \ \theta_0, \lambda_{ij}) \times \alpha_g(\theta_0, \lambda) K(\lambda_{ij}) F(\lambda_{ij}). \tag{6}$$

From (3) and (6) we easily obtain the sample roughness spectrum in function of the ratio between the signals delivered by the etalon and the sample,

$$\gamma(i, \theta_0, \lambda_{ij}) = \frac{S_s(i, \theta_0, \lambda_{ij})}{S_L(\theta_0, \lambda_{ij})} \left(\frac{\cos\theta_0}{\pi}\right) (1 - A)/C(i, \theta_0, \lambda_{ij}). \tag{7}$$

At normal illumination ($i = 0°$), we obtain

$$\gamma(\theta_0, \lambda_{ij}) = \frac{S_s(\theta_0, \lambda_{ij})}{S_L(\theta_0, \lambda_{ij})} \left(\frac{\cos\theta_0}{\pi}\right) (1 - A)/C(\theta_0, \lambda_{ij}). \tag{8}$$

As we already mentioned, the light is not polarized in this experiment, and we work in the incidence plane. Therefore, the optical coefficient C will be expressed as $C = \frac{1}{2} \ (C_{ss} + C_{pp})$, where C_{ss} is the coefficient in s polarization and C_{pp} is the coefficient in p polarization [7,10,23]. At this step, measurements can be proceeded: the two signals (S_s and S_L) are measured, the etalon absorption ($<10^{-2}$) is known, and the optical factor is calculated versus wavelength. Note that the achromatic dispersion of substrate materials can be taken into account when necessary.

4. MEASUREMENTS

The next goal is to validate the technique. For these first measurements, the detectivity of the instrument is not optimized and that is why we choose samples that are not too low in scattering, whereas remaining within the framework of the first-order approximation (low roughness-to-wavelength ratio). We considered two types of samples. The first is the non-super-polished face of a silicon wafer, which is around 10-nm roughness. The second is a polished black glass sample (around 1-nm roughness) that we coated with 200 nm of aluminum (Al); the reason for this Al coating is to increase the scattering (by a factor of >20), whereas, we know that the Al layer reproduces the glass roughness [1,2]. Note that the two samples are opaque so that the whole scattering originates from their front surfaces that we characterize.

For these experiments the scattering direction is $\theta_0 = 30°$. For each measurement, the integration time, that can be composed between 3 ms and 7 s, is adjusted to avoid saturation of the spectrometer, which intervenes at 65000 counts. In Fig. 4, we give the broadband scattering from the Lambertian etalon and from the Si sample under test. The wavelength range is 490 nm–905 nm. Due to the absence of chromatic coatings, the curves look similar in shape. The ratio of these two curves gives the roughness spectrum of the Si sample plotted in Fig. 5. The same data were recorded for the Al sample, whose roughness spectrum is also plotted in Fig. 5. For better accuracy, the

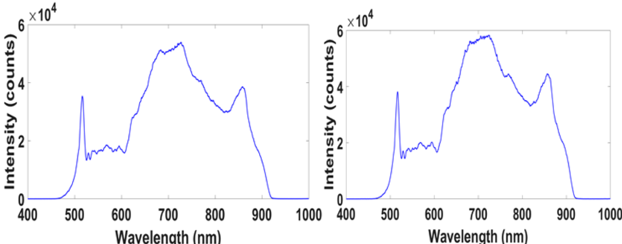

Fig. 4. White signals measured by the spectroscatterometer after scattering on the silicon sample (left, integration time is 900 ms) and on the Lambertian sample (right, integration time is 8 ms) for a detector placed at 30°.

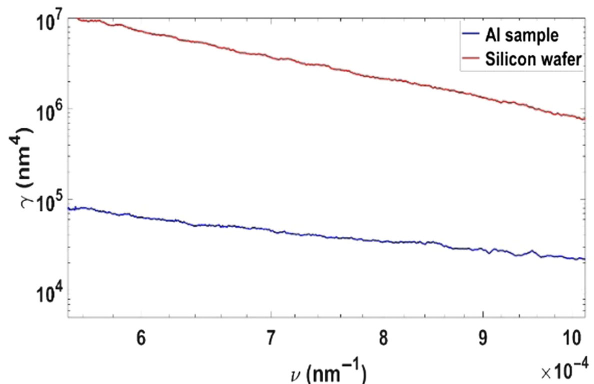

Fig. 5. Roughness spectra determined for the Si sample and the Al sample.

complex index dispersion of Si and Al was considered [26] in the calculation of the C factor involved in relation (8). We observe that the Al spectrum exhibits a lower slope and a lower amplitude. Integration of these spectra gives the roughness in the bandwidth of measurements (see the next section) [7,27,28]. The result is $\delta_{Si} = 3.7$ nm and $\delta_{Al} = 0.2$ nm corresponding to this range of spatial frequencies. Note that these values are lower than those that would be obtained with a classical angle-resolved setup (see the next section) because of a narrower bandwidth. Expanding the bandwidth would, however, be possible using a source with a wider wavelength range.

5. CONSISTENCY OF RESULTS

As is often the case, given that this system is entirely new, it is interesting to carry out different tests to check the consistency and compliance of the results. The roughness values could be first compared to those issued from a classical ARS [16–19]. However, there is also another key test to test the procedure itself and the principles, which consists of the exploration of different bandwidths in which the spectra would overlap at their intersections [24,27,28].

For that we change the scattering direction θ_0 and iterate the results for a series of angles θ_0. Since the bandwidth is given by BW $(\theta_0) = \left[\frac{\sin(\theta_0)}{\lambda_{max}}; \frac{\sin(\theta_0)}{\lambda_{min}}\right]$ with λ_{min} and λ_{max} the minimum and maximum wavelengths, this bandwidth is modified for each angle θ_0. Hence, with this procedure, one can measure the scattering signals in different bandwidths that overlap, and the key

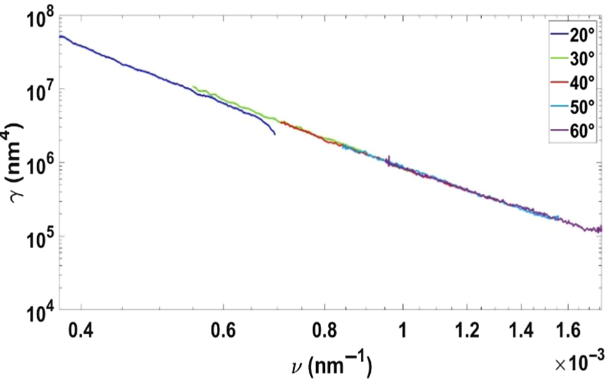

Fig. 6. Roughness spectra measured for the silicon wafer in different bandwidths, that is, for different positions of the detector.

point is to check that all roughness spectra overlap at the intersection of bandwidths [24,27,28]. In other words, this means that we measure the spectrum at the same spatial frequency $[\nu \sim \sin(\theta_0)/\lambda]$, but at a different angle and wavelength.

In our setup, the extreme wavelengths are the limits of the recorder spectrum. In our case, we have $\lambda_{min} = 490$ nm and $\lambda_{max} = 905$ nm, these limits being determined by the spectral response of the spectrometer. They could be expanded by the use of spectrometers with broader range. Consequently, the spectra will be slightly shifted in terms of spatial frequencies when the angle of detection is changed.

We show in Fig. 6 the roughness spectra measured on the silicon wafer for five different angles composed between $\theta_0 = 20°$ and $\theta_0 = 60°$. We observe that the shifted spectra at different angles all recover well so that the results are rather successful. It is interesting to stress that the complex index dispersion of Si is necessary to ensure the overlapping of spectra. Note that the total range of spatial frequencies that we can access here is $[0.4\ 10^{-3}\ \text{nm}^{-1}$ and $1.7\ 10^{-3}\ \text{nm}^{-1}]$, which corresponds approximately to the measurement range of a classical ARS. Eventually, if we integrate the roughness spectrum in this range, we obtain a roughness value of 9 nm, in good agreement with the expected value for the nonpolished face of a silicon wafer.

The same procedure was operated for the Al sample. Recall that this is a glass sample coated with 200 nm of Al so that it is opaque in our wavelength range. In this manner, we cancel potential effects due to the transparency or fluorescence of the glass. For a better precision, we included in our calculation the spectral dispersion of the real and imaginary parts of the index of Al. This condition is necessary to reach good overlapping of spectra. Results are plotted in Fig. 7. Although they are again satisfying, we note a slight offset. It could be explained by the presence of impurities, such as dusts remaining on the surface that disturb the spectra and that have more influence when the roughness is low [13,29]. The small oscillations on the spectra are consistent with this hypothesis as this type of signal is typically generated by these defects. This slight offset could also originate from bulk scattering, luminescence, or from uncertainties in the dispersion law of Al.

The integrated value of roughness obtained on the whole range is 0.5 nm, which is a satisfactory value for an Al-coated polished glass sample.

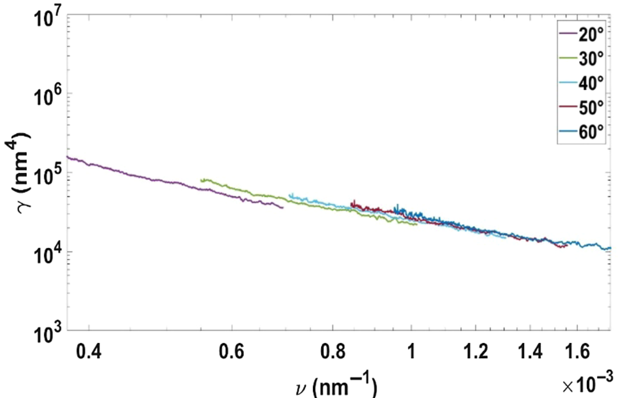

Fig. 7. Roughness spectra measured for the Al sample in different bandwidths, that is, for different positions of the detector.

To conclude this section, it should be noted that we have used several angles in order to check the consistency of the results. With all these angles, the bandwidth of the white-light setup is obviously similar to that of a classical ARS setup. But, in general, the white-light setup is not intended to be used at several angles. The bandwidth will, therefore, be reduced, unless the wavelength range is widened as outlined at the end of the previous section.

6. CONCLUSION

Extending previous studies on motionless scatterometers based on the use of white light [20,21], we proposed a new method that we believed is superior for most situations. The setup was very simple as it mainly required only a broadband illumination source and a spectrometer (both were commercially available) to analyze light scattering at a unique direction. Spectral shaping of the illumination beam was not required with the new method, which simplified implementation. Furthermore, we have direct access to the roughness spectrum, instead of the roughness moments of the previous version. This made easier the comparison with other existing ARS scatterometers.

After calibration with a Lambertian sample, the method was validated with measurements performed on two samples, a silicon wafer (9-nm roughness) and a black glass sample overcoated with Al (0.5 nm). In order to check the consistency of results, we modified the scattering direction to shift the frequency bandwidths. The roughness spectra showed an excellent overlap at the intersection of bandwidths, which proved a successful test. Furthermore, the integrated values of roughness were in good agreement with the expected values for each type of sample.

This setup, thus, provided instantaneous measurements of the surface roughness spectra with a simple and flexible experiment. As in the case of the previous motionless white-light scatterometers, the new method provided results over a reduced range of spatial frequencies as compared to those of angle-resolved scatterometers [18]. To extend the range, it was possible to use spectrometers with a wider spectral response, which were also commercially available. For instance, the spectrometers from WASATCH PHOTONICS were able to cover the ranges [250 nm and 1600 nm]. In all cases, the technique will be of great use for samples that cannot be moved.

Funding. Agence Nationale de la Recherche (ANR-19-CE42-0009).

Disclosures. The authors declare no conflicts of interest.

Data availability. The datasets presented in this paper are available from the corresponding author upon reasonable request.

REFERENCES

1. C. Amra, "Light-scattering from multilayer optics. 1. Tools of investigation," J. Opt. Soc. Am. A **11**, 197–210 (1994).
2. C. Amra, "Light-scattering from multilayer optics. 2. Application to experiment," J. Opt. Soc. Am. A **11**, 211–226 (1994).
3. S. O. Rice, "Reflection of electromagnetic waves from slightly rough surfaces," Commun. Pure Appl. Math. **4**, 351–378 (1951).
4. J. M. Eastman, "Surface scattering in optical interference coatings," J. Opt. Soc. Am. **66**, 164 (1976).
5. J. M. Bennett and L. Mattsson, *Introduction to Surface Roughness and Scattering* (Optical Society of America, 1989).
6. J. C. Stover, *Optical Scattering: Measurement and Analysis*, 3rd ed. (SPIE, 2012).
7. C. Amra, M. Lequime, and M. Zerrad, *Electromagnetic Optics of Thin-Film Coatings* (Cambridge University, 2021).
8. C. Amra, J. H. Apfel, and E. Pelletier, "Role of interface correlation in light-scattering by a multilayer," Appl. Opt. **31**, 3134–3151 (1992).
9. P. Roche and E. Pelletier, "Characterization of optical surfaces by measurement of scattering distribution," Appl. Opt. **23**, 3561–3566 (1984).
10. J. M. Elson, J. M. Bennett, and J. C. Stover, "Wavelength and angular dependence of light scattering from beryllium: comparison of theory and experiment," Appl. Opt. **32**, 3362–3376 (1993).
11. P. Kadkhoda, A. Müller, D. Ristau, A. Duparré, S. Gliech, H. Lauth, U. Schuhmann, N. Reng, M. Tilsch, R. Schuhmann, C. Amra, C. Deumie, C. Jolie, H. Kessler, T. Lindstrm, C.-G. Ribbing, and J. M. Bennett, "International round-robin experiment to test the international organization for standardization total-scattering draft standard," Appl. Opt. **39**, 3321–3332 (2000).
12. A. Duparré, J. Ferre-Borrull, S. Gliech, G. Notni, J. Steinert, and M. Bennett, "Surface characterization techniques for determining the root-mean-square roughness and power spectral densities of optical components," Appl. Opt. **41**, 154–171 (2002).
13. M. Lequime, M. Zerrad, C. Deumié, and C. Amra, "A goniometric light scattering instrument with high-resolution imaging," Opt. Commun. **282**, 1265–1273 (2009).
14. S. Schröder, D. Unglaub, M. Trost, X. B. Cheng, J. L. Zhang, and A. Duparre, "Spectral angle resolved scattering of thin film coatings," Appl. Opt. **53**, A35–A41 (2014).
15. M. Zerrad, M. Lequime, and C. Amra, "Far-field spatially angle-resolved scattering measurements: practical way to recover surface topography," Opt. Eng. **53**, 092012 (2014).
16. M. Lequime, S. Liukaityte, M. Zerrad, and C. Amra, "Ultra-wide-range measurements of thin-film filter optical density over the visible and near-infrared spectrum," Opt. Express **23**, 26863–26878 (2015).
17. M. Lequime, M. Zerrad, and C. Amra, "Breakthrough spectrophotometric instrument for the ultra-fine characterization of the spectral transmittance of thin-film optical filters," Opt. Express **26**, 34236–34249 (2018).
18. M. Fouchier, M. Zerrad, M. Lequime, and C. Amra, "Wide-range wavelength and angle resolved light scattering measurement setup," Opt. Lett. **45**, 2506–2509 (2020).
19. S. Liukaityte, M. Lequime, M. Zerrad, T. Begou, and C. Amra, "Broadband spectral transmittance measurements of complex thin-film filters with optical densities of up to 12," Opt. Lett. **40**, 3225–3228 (2015).
20. C. Amra, M. Zerrad, S. Liukaityte, M. Lequime, and M. Zerrad, "Instantaneous one-angle white-light scatterometer," Opt. Express **26**, 204–219 (2018).
21. X. Buet, M. Zerrad, M. Lequime, G. Soriano, J.-J. Godeme, and C. Amra, "Immediate and one-point roughness measurements using spectrally shaped light," Opt. Express **30**, 16078–16093 (2022).
22. R. A. Probst, T. Steinmetz, T. Wilken, G. K. L. Wong, H. Hundertmark, S. P. Stark, P. S. J. Russell, T. W. Hänsch, R. Holzwarth, and T. Udem,

"Spectral flattening of supercontinua with a spatial light modulator," Proc. SPIE **8864**, 88641Z (2013).

23. C. Amra, D. Torricini, and P. Roche, "Multiwavelength (0.45-10.6-Mu-M) angle-resolved scatterometer or how to extend the optical window," Appl. Opt. **32**, 5462–5474 (1993).
24. S. Schroder, M. Trost, T. Herffurth, A. von Finck, and A. Duparre, "Sophisticated light scattering techniques from the VUV to the IR regions," in *Reflection, Scattering, and Diffraction from Surfaces III*, L. M. Hanssen, ed. (2012), Vol. **8495**.
25. C. Amra, C. Grézes-Besset, and L. Bruel, "Comparison of surface and bulk scattering in optical multilayers," Appl. Opt. **32**, 5492–5503 (1993).
26. https://refractiveindex.info/.
27. P. Dumas, B. Bouffakhreddine, C. Amra, O. Vatel, E. Andre, R. Galindo, and F. Salvan, "Quantitative microroughness analysis down to the nanometer scale," Europhys. Lett. **22**, 717–722 (1993).
28. C. Deumié, R. Richier, P. Dumas, and C. Amra, "Multiscale roughness in optical multilayers: atomic force microscopy and light scattering," Appl. Opt. **35**, 5583–5594 (1996).
29. S. Maure, G. Albrand, and C. Amra, "Low-level scattering and localized defects," Appl. Opt. **35**, 5573–5582 (1996).

194.199.107.6 {ts '2023-03-24 11:51:40'}